Dynamical model development and parameter identification for solid-state anaerobic digestion of shellfish products: Application to Mytilus edulis

A. Coutu, D. Dochain, S. Mottelet, L. André, M. Mercier-Huat, A. Pauss, T. Ribeiro

Dynamical model development and parameter identification for solid-state anaerobic digestion of shellfish products: Application to *Mytilus edulis*

A. Coutu[a], D. Dochain[b], S. Mottelet[c], L. André[a], M. Mercier-Huat[a], A. Pauss[c], T. Ribeiro[a*]

[a]Institut Polytechnique UniLaSalle, Université d'Artois, ULR 7519, 19 Rue Pierre Waguet, BP 30313, 60026 Beauvais, France

[b]Université Catholique de Louvain, Mathematical Engineering department (INMA), 4-6 avenue Georges Lemaître, B-1348 Louvain-la-Neuve, Belgium

[c]Université de Technologie de Compiègne, ESCOM, TIMR (Integrated Transformations of Renewable Matter), Centre de recherche Royallieu - CS 60 319 - 60 203 Compiègne Cedex

*Corresponding author: Thierry Ribeiro; Tel.: +33 (0) 344 06 76 11; E-mail: thierry.ribeiro@unilasalle.fr

Abstract

A simplified AM2 model was developed to characterize mussel solid-state anaerobic digestion. This model considers two different substrates for mussels' degradation: the mussel meat and the mussel juice obtained after sanitization. This model was implemented to characterize the anaerobic degradation of *Mytilus edulis* species. This model was verified, implemented, and validated in 60L batch reactors in mesophilic conditions. Two different experiments were used to calibrate kinetics using reaction invariants and an interior point optimization method. A conditioning study and a sensitivity analysis were done and had shown a better sensitivity with delayed substrate injections throughout the experiment with a factor of 10. An 88.6% accumulation of methane yield of the BMP measurement was observed, corresponding to 57.7% volatile removal with a minimum mass balance of 96.1%. Additionally, the model proposed in this study was able to successfully predict the two characteristic methane yield peaks observed during solid-state anaerobic digestion.

Keywords

Anaerobic digestion; Mathematical modeling; Sensitivity analysis; Inhibition; Kinetic parameters

1 Introduction

Shellfish aquaculture consists of domestic shellfish farming by humans. Mussels are among the most popular farmed shellfish in the world, with an increasing worldwide production of over 2 million tonnes per year, with China, Chili, and Spain as the main producers (FAO, 2020). *Mytilus edulis*, otherwise known as blue mussels, is the third more farmed species after *Mytilus galloprovincialis* and *Mytilus chilensis* with over 10 % of global mussel production. France is one of the main producers of this last species with an annual production of 47,000 t (FAO, 2020). However, only 660 $kg.t^{-1}$ is suitable for human consumption (Vareltzis and Hundeland, 2012), resulting in a large amount of waste that could be valued. Many parts of the mussel could indeed be used: byssal thread, shell, and mussel meat are sources of fat, protein, carbohydrates, and other bioactive compounds. These by-products from mussel wastes could be valorized as functional ingredients for animals (Sardenne *et al*., 2019; Afrose *et al*., 2016) or humans (Vijaykrishnaraj *et al*., 2016; Zhang *et al*., 2013), as building material (Martínez-Garcia *et al*., 2020; Martínez-Garcia *et al*., 2019) or as soil improvement to improve soil fertility and microbial activity (Fernandez-Calviño *et al*., 2018; Messiga *et al*., 2016) or soil decontamination (DiLoreto *et al*., 2016; Fernandez-Calviño *et al*., 2015; Seco *et al*., 2014). Compounds of chemical interest could be extracted from mussel wastes as bioactive proteins, polyunsaturated fatty acids, enzymes, mineral compounds, or pigments (Naik and Hayes, 2019; Pintado *et al*., 1999). Another way to valorize mussel wastes is anaerobic digestion (AD). AD is a biological process that consists of the degradation of an organic substrate by a microbial consortium to produce biogas and digestate. This process kinetics may be divided into 4 main steps which are hydrolysis, acidogenesis, acetogenesis, and methanogenesis (Kothari *et al*., 2014; Li *et al*., 2011; Amani *et al*., 2010). Solid-state anaerobic digestion (SS-AD) is defined by a

total solid content higher than 15 % and is less common in industrial applications but is more efficient in the digestion of high solid content feedstock like cattle manure or corn silage (Karthikeyan and Visvanathan, 2013; André *et al*., 2018). This approach reduces the reactor size, the amount of water used, and thus the amount of energy required. However, many scientific challenges still exist in this process due to the lack of knowledge on SS-AD including local accumulation of inhibitors as volatile fatty acids (VFA) due to the medium heterogeneity (André *et al*., 2018).

AD of *Mytilus edulis* have already been implemented (Wollak *et al*., 2018; Akizuki *et al*., 2018) with great methane yield between 310 $m^3.t_{VS}^{-1}$ and 490 $m^3.t_{VS}^{-1}$ using one-step and two-step processes. Other studies showed that optimal conditions are reached when alkalinity is controlled (Murto *et al*., 2004). Concerning *Mytilus edulis*, the salt concentration is an important parameter to guarantee optimal methane production and avoid process inhibitions (Zhang *et al*., 2017; Anwar *et al*., 2016; Kimata-Kino *et al*., 2011). *Mytilus edulis* SS-AD was already carried out in an Upflow Anaerobic Sludge Blanket (UASB) with a methane yield of 330 $m^3.t_{VS}^{-1}$ (Nkemka and Murto, 2013) attesting the SS-AD feasibility while maintaining process efficiency, but the digestion of mussels including shells gave low methane production. A better understanding of the phenomenon is necessary to provide a better degree of predictability regarding methane production. Mathematical modeling can be a useful understanding tool for representing biological kinetics through equations (Du *et al*., 2021; Fdez.-Güelfo *et al*., 2011). This understanding could help to implement some prediction and control tools to optimize methane production for SS-AD (Zhou *et al*., 2020; Donoso-Bravo *et al*., 2011). Different SS-AD models were developed in the literature (Coutu *et al*., 2022; Xu *et al*., 2015) including modeling of perfectly mixed systems using ordinary differential equation systems (ODE) to reach a compromise between the model complexity and the kinetic parameters identifiability as the AM2 model (Bernard *et al*., 2001). The current models of

anaerobic digestion are simple models such as the Gompertz model, perfectly mixed models such as the ADM1 model and its derivatives, heterogeneous models such as the distributed model and its derivatives for solid-state anaerobic digestion, and statistical models such as the logistical model (Liu *et al*., 2023). However, no model available in the literature is adapted to a substrate such as *Mytilus edulis* due to the complexity of its degradation. Indeed, the degradation of the mussel and the released juice of the mussel with the risks of inhibitions that this implies cannot be simply modeled using the models available in the literature. This study aimed to mathematically develop an innovative modified AM2 model to characterize complex substrates SS-AD such as *Mytilus edulis* SS-AD. This model was verified, implemented, and validated in 60L batch reactors in mesophilic conditions using the asymptotic observers' method, which is not used much in the literature and is yet a very practical method to obtain as much experimental information as possible from the measurements made.

2 Materials and methods

2.1 Physicochemical characterization of substrate and inoculum

Undersize *Mytilus edulis* mussels (MeM) used for SS-AD were sampled from the CultiMer France workshop (Vivier-sur-Mer, France). These mussels were separated and crushed (with a thickness of 12 mm) from marketable bouchot mussels with a mussel sizer and a grinder on the sorting line, randomly sampled and transported to the UniLaSalle Polytechnic Institute (Beauvais, France). A sanitizing step during 1h at 70°C (Klarstein 60L, Germany) was realized. During these operations, mussels released a liquid called released juice (RJ) which was considered a different substrate than mussels during SS-AD. Liquid bovine manure (LM) was sampled from the farm of the UniLaSalle Polytechnic Institute (Beauvais, France) and was used as *inoculum* to bring the microbial consortium. LM was filtered by a mesh with 5 mm diameter holes to avoid solid clogging in the recirculation pipe.

The total solid content (TS) and the volatile solid (VS) content of MeM, RJ, and *inoculum* were determined by a 105°C drying for 24h and combustion at 550°C for 2h (APHA, 1988). The pH was measured with a pH meter (Mettler Toledo, Switzerland), and the total volatile fatty acid content (VFA) and the buffer capacity (TAC) were determined with an automatic titrator (Mettler Toledo, Switzerland) by two titrations using sulfuric acid. For VFA/TAC measurement, samples were centrifuged at 9000 rpm for 20 min to remove the micro-organisms which could induce an intracellular content release. Chemical Oxygen Demand (COD), Ammonium concentration, Calcium, Sodium, and total Nitrogen concentration were determined using WTW kits (WTW, Germany). All measures have been triplicated. The biochemical methane potential (BMP) of each substrate was measured using an AMPTS I device (Automatic Potential Test System, Bioprocess Control, Sweden) according to Holliger et al. (2016). All the results are reported in **Table 1**.

2.2 Experimental set-up

Two batch reactors made of polyethylene with a total volume of 60 L (considering a 50 cm height and a 39 cm diameter) were used for one run of experiments under mesophilic conditions. Experiments are (R1) and (R2). Each reactor was equipped with a plastic holder to separate the liquid and the solid phases. The reaction process took place in the liquid phase. A grid with holes of 5 mm diameter was placed on the plastic holder to avoid solid blockages due to pieces of shells in the recirculation pipe. The liquid phase composed of inoculum and RJ was recirculated in each reactor with an external peristaltic pump (Masterflex, USA) respecting a liquid flow rate of 15 $L.h^{-1}$, for 15 min each hour. Thus, the liquid phase was spread out across the top of the solid phase inside the reactor. Each reactor was connected to a biogas flow counter (Drum gas meter TG05, Ritter, Germany), and biogas production was continuously measured and daily averaged. The biogas composition was daily measured with a biogas analyzer (MGA300 multi-gas analyzer ADC gas

118 analysis Ltd., Hoddesdon United Kingdom) and manually verified with a portative biogas analyzer
119 (Multitec 540 Sewerin, Germany) to avoid measurement drift due to daily recalibration.

120 RJ brings a non-negligible quantity of volatile content which contributed to VFA accumulation and
121 could cause biological inhibitions (Karthikeyan and Visvanathan, 2013; Siegert and Banks, 2005). To
122 study the RJ impact on MeM SS-AD, different addition strategies were adopted on each reactor.
123 The inoculum/substrate ratio was similar in the two experimented conditions (I/S=0.41) to
124 compare the experimental results. Each reactor was filled with 12 kg of MeM and 23 kg of LM. RJ
125 was added in each reactor following a different strategy for each reactor: 3.5 kg of RJ was placed
126 inside the first reactor (R1) at the beginning of the experiment and 5 constant additions of 0.7 kg of
127 RJ were made in the second reactor (R2) during day 4, day 7, day 10, day 14, and day 17 with a
128 ratio I/S=0.41.

129 Once these reactors were filled, each of them was sealed and the temperature was held at a
130 constant value of 37°C with a thermostatically controlled water bath for each experiment for 41
131 days. Each experiment is described in **Fig 1**. At the end of each experiment, mass balances were
132 determined.

133 ### *2.3 Mathematical model implementation*

134 #### *2.3.1 Modeling assumptions*

135 Let us first consider the following assumptions for the derivation of the dynamical model of the
136 process. First of all, all the state variables are expressed in COD units, and in consequence carbon
137 dioxide does not appear in the model because it could not be oxidized. Moreover, the
138 disintegration, hydrolysis, and acidogenesis steps have been gathered in a single step named DHA
139 and modeled by first-order kinetics as proposed in Bollon *et al*. (2011). This assumption could be
140 made because MeM and RJ are mostly composed of proteins, lipids, and carbohydrates whose

hydrolysis is the limiting step. In addition, the acidogenic step is very fast in comparison with the hydrolysis step. Instead of different volatile fatty acids, only a generic equivalent acetic acid was considered (Bernard *et al*., 2001). As a consequence, the acetogenesis step was removed from the model. These assumptions allow us to reduce the number of parameters to be determined. Regarding biomass growth, the methanogenic biomass is assumed to be constant, which means that microbial growth and death are neglected. Indeed, less than 10% of the organic part of substrates is turned into biomass (Batstone *et al*., 2002) and this assumption allows us to identify the kinetic parameters. Ammonia was not considered in this model because there was always a very constant concentration of ammonia in all measurements. Hydrogen is an intermediate gas in SS-AD and its concentration is negligible, therefore hydrogen was not considered either. Methane was assumed to have negligible solubility in the liquid phase and therefore the methane liquid-gas transfer was neglected to simplify the model. Finally, RJ was supposed more easily degradable than MeM due to the solutes' accessibility, and all the organic substrate entering the batch reactor was assumed fully biodegradable.

2.3.2 Anaerobic digestion model and reaction kinetics

A three-reaction-based biological kinetic model scheme was used for this study to provide a simple and understandable representation of the phenomenon. In this model, the DHA biomass (X_1) hydrolyses and converts MeM (S_1^1) and RJ (S_1^2) into VFA (S_2) during the DHA step. Then VFA is converted into methane (CH_4) during the methanogenesis step. The following equations present the model reactions:

DHA - MeM $$S_1^1 \xrightarrow{r_1^1} k_1^1 S_2 + (1 - k_1^1) X_1 \quad \textbf{(1)}$$

DHA - RJ $$S_1^2 \xrightarrow{r_1^2} k_1^2 S_2 + (1 - k_1^2) X_1 \quad \textbf{(2)}$$

Methanogenesis $S_2 \xrightarrow{r_2} k_2 CH_4$ **(3)**

A first-order kinetic was used for DHA steps, and a Haldane kinetic model with acid concentration inhibition was used to consider for methanogenesis step for the accumulated methane yield. k_1^1 and k_1^2 represent respectively the acidogenesis and methanogenesis conversion rates, $(1-\mathrm{k}_1^1)$ and $(1-\mathrm{k}_1^2)$ represent respectively the acidogenesis biomass and methanogenesis biomass growth rates. A Peterson matrix summarizes these kinetics in **Table 2**. In this table, μ_1^1 represents the DHA rate of X_1 other S_1^1, μ_1^2 represents the DHA rate of X_1 other S_1^2, K_{S2} represents the half-saturation constant associated with S_1^1 and S_1^2, $\mu_2^{\max}$ represents the maximum growth rate of X_2 other S_2 and K_I is the inhibition constant associated with the consumption of S_2. The dynamical system obtained for mesophilic SS-AD is composed of 5 ordinary differential equations (ODE):

$$\frac{dS_1^1}{dt} = -\mathrm{r}_1^1 \quad \textbf{(4)}$$

$$\frac{dS_1^2}{dt} = -\mathrm{r}_1^2 \quad \textbf{(5)}$$

$$\frac{dS_2}{dt} = \mathrm{k}_1^1\mathrm{r}_1^1 + \mathrm{k}_1^2\mathrm{r}_1^2 - r_2 \quad \textbf{(6)}$$

$$\frac{dX_1}{dt} = (1-\mathrm{k}_1^1)\mathrm{r}_1^1 + (1-\mathrm{k}_1^2)\mathrm{r}_1^2 \quad \textbf{(7)}$$

$$\frac{dCH_4}{dt} = k_2 r_2 \quad \textbf{(8)}$$

2.3.3 State variables initialization

There are 5 state variables in the model, a lower number than other models of the literature as the ADM1 (Batstone *et al*., 2002) and modified solid-state models (Bollon *et al*., 2011; Abbassi-Guendouz *et al*., 2012; Coutu *et* al., 2022), due to the previous assumptions. The total COD of LM,

MeM (S_1^1), and RJ were measured. RJ contained initial VFA extracted from mussels during sanitizing. This is why COD of RJ was divided into initial VFA (S_2^0) and initial RJ (S_1^2). Initial VFA content was measured and initial RJ was deduced from this value. The COD of biomass was divided into DHA biomass (X_1) and methanogenic biomass (X_2) respecting a 25%-75 % ratio according to Gavala et al. (2003). X_2 was supposed to be constant all along SS-AD per the modeling assumptions.

2.3.4 Mass balance model

A total mass balance and a first simulation were led to perform a model validation of the initialization conditions and during calibration and validation steps. This step allows us to verify mass conservation. The total mass balance expressed in equation (9) meets equation (10).

$$Total\ mass\ balance = S_1^1 + S_1^2 + S_2 + CH_4 \quad \textbf{(9)}$$

$$\frac{dS_1^1}{dt} + \frac{dS_1^2}{dt} + \frac{dS_2}{dt} + \frac{dCH_4}{dt} = 0 \quad \textbf{(10)}$$

2.4 Computational aspects

2.4.1 Calibration and Validation steps

Calibration was performed on the experiment (R2) for which RJ was added at constant intervals with constant amounts. This procedure allowed us to generate data that better scan the kinetics curves. 7 stages were identified in this experiment: stage 1 represents the period during which only MeM was consumed and RJ was absent from the reactor. Stages 2 through 6 represent the periods between each RJ addition. Finally, stage 7 represents the period during which all the RJ and the MeM were consumed and only the remaining VFA was consumed. The identification of these different stages allowed us to determine the kinetic parameters of the DHA step and the

195 monitoring of unmeasured state variables as presented in section 2.4.3. The validation step was
196 conducted on the experiment (R1) for which all RJ was injected into the reactor at the beginning of
197 the experiment. The cumulative methane production, the methane flow rate, and the VFA
198 concentration were then compared with the simulated values to validate the calibration step. 2
199 periods were identified in the first experiment (R1): a first stage of rapid consumption of RJ with a
200 little degradation of MeM, and a second stage during which only the remaining MeM was
201 consumed. The kinetic parameters of the DHA were also determined in this experiment to validate
202 the values obtained during the calibration step.

203 *2.4.2 Identifiability of model parameters and unmonitored variables*

204 The notion of reaction invariants (Dochain and Vanrolleghem, 2001) allows writing a part of
205 process dynamics independently of the reaction kinetics. This property is very helpful when one or
206 more variables are not accessible for measurement. Reaction invariants rely on the mass balance
207 or part of the mass balance to determine the concentration of one or more of the solutes in the
208 process. This method is applied in this part to determine hydrolysis parameters k_1^1 and k_1^2 and
209 substrate concentrations S_1^1 and S_1^2.

210 *2.4.2.1 Hydrolysis parameters determination*

211 The yield constants k_1^1 and k_1^2 were first identified during the anaerobic digestion. For this, the
212 periods during which only MeM was consumed allowed to determine the constant k_1^2 while the
213 periods for which both substrates were consumed allowed to determine k_1^1. Two assumptions
214 were made to use the reaction invariant method:

215 • The methanogenesis step is the limiting kinetic step
216 • The methane produced in aqueous form is instantaneously transferred to the gas phase

These assumptions resulted in a k_2 constant and $\frac{dCH_{4,L}}{dt} = 0$. The reaction invariant used for the determination of k_1^1 is Z_2 defined in equation (11). Based on the assumptions presented above, equations (12), (13), and (14) were obtained and the coefficient k_1^2 was calculated by integration from the experimental data.

$$Z_2 = k_1^2 S_1^2 + FOS + \frac{CH_{4,l}}{k_2} \quad \textbf{(11)}$$

$$\frac{dZ_2}{dt} = k_1^2 \frac{dS_1^2}{dt} + \frac{dFOS}{dt} = -r_2 = -\frac{Q_{CH4}}{k_2} \quad \textbf{(12)}$$

$$k_1^2 \int_{S_1^{2,i}}^{S_1^{2,f}} dS_1^2 + \int_{FOS^i}^{FOS^f} dFOS = -\frac{1}{k_2} \int_{t^i}^{t^f} Q_{CH4} dt \quad \textbf{(13)}$$

$$k_1^2 = -\frac{\left(CH_{4,g}^f - CH_{4,g}^i\right) + k_2(FOS^f - FOS^i)}{k_2\left(S_1^{2,f} - S_1^{2,i}\right)} \quad \textbf{(14)}$$

Knowing the value of k_1^2, the same method was applied over the periods during which both substrates were consumed to determine k_1^1. The considered reaction invariant Z_1 is presented in equation (15). Under the assumptions made earlier, equations (16), (17), and (18) were obtained. k_1^1 was then determined by integration from the experimental data. Results are presented in **Table 3**.

$$Z_1 = k_1^1 S_1^1 + k_1^2 S_1^2 + FOS + \frac{CH_4}{k_2} \quad \textbf{(15)}$$

$$\frac{dZ_1}{dt} = k_1^1 \frac{dS_1^1}{dt} + k_1^2 \frac{dS_1^2}{dt} + \frac{dFOS}{dt} = -\frac{Q_{CH4}}{k_2} \quad \textbf{(16)}$$

$$k_1^1 \int_{S_1^{1,i}}^{S_1^{1,f}} dS_1^1 + k_1^2 \int_{S_1^{2,i}}^{S_1^{2,f}} dS_1^2 + \int_{FOS^i}^{FOS^f} dFOS = -\frac{1}{k_2} \int_{t^i}^{t^f} Q_{CH4} dt \quad \textbf{(17)}$$

$$k_1^1 = -\frac{\left(CH_{4,g}^f - CH_{4,g}^i\right) + k_1^2\left(S_1^{2,f} - S_1^{2,i}\right) + k_2(FOS^f - FOS^i)}{k_2\left(S_1^{1,f} - S_1^{1,i}\right)} \quad \textbf{(18)}$$

226 *2.4.2.2 Unmonitored state variables tracking with asymptotic observers*

227 The method of reaction invariants was also used to determine the evolution of unmeasured state
228 variables. For this, the property of reaction invariants was used to estimate their value and to
229 deduce the state variable values as a function of time. Thus, the reaction invariant Z_2 was
230 estimated to determine the evolution of S_1^2 during periods when only MeM was consumed and the
231 reaction invariant Z_1 was estimated to determine S_1^1 during periods when both substrates were
232 consumed. The expressions presented in equations (19) and (20) allowed the estimation of Z_1 and
233 Z_2 considering the concentration of methane gas. The expression of these two reaction invariants
234 allowed us to deduce the curve shapes of S_1^2 and S_1^1 using equations (21) and (22).

$$\widehat{Z_2} = k_1^2 S_1^{2,t} + FOS^t + \frac{CH_{4,g}^t}{k_2} \quad \textbf{(19)}$$

$$\widehat{Z_1} = k_1^1 S_1^{1,0} + k_1^2 S_1^{2,0} + FOS^0 + \frac{CH_{4,g}^0}{k_2} \quad \textbf{(20)}$$

$$\widehat{S_1^2} = \frac{1}{k_1^2}\left(\widehat{Z_2} - FOS - \frac{CH_{4,g}}{k_2}\right) \quad \textbf{(21)}$$

$$\widehat{S_1^1} = \frac{1}{k_1^1}\left(\widehat{Z_1} - FOS - \frac{CH_{4,g}}{k_2} - k_1^2 S_1^2\right) \quad \textbf{(22)}$$

2.4.2.3 DHA kinetic parameters determination

The kinetic parameters of the DHA step for RJ and MeM were determined differently. Indeed, the experimental S_0 concentration was known at the beginning and the end of the experimental data set and allowed us to integrate the DHA first-order kinetics to directly determine μ_1^1 and μ_1^2 according to equations (23) and (24). Results are presented in **Table 3**.

$$\begin{cases} \frac{dS_1^1}{dt} = -\mathrm{r}_1^1 = -\mu_1^1 S_1^1 X_1 \\ \frac{dS_1^2}{dt} = -\mathrm{r}_1^2 = -\mu_1^2 S_1^2 X_1 \end{cases} \quad \textbf{(23)}$$

$$\begin{cases} \mu_1^1 = \dfrac{\ln\left(\frac{S_1^1(t=t_i)}{S_1^1(t=t_f)}\right)}{\int_{t_i}^{t_f} X_1 dt} \\ \mu_1^2 = \dfrac{\ln\left(\frac{S_1^2(t=t_i)}{S_1^2(t=t_f)}\right)}{\int_{t_i}^{t_f} X_1 dt} \end{cases} \quad \textbf{(24)}$$

2.4.2.4 Haldane kinetic parameters determination

In practice, it is difficult to obtain the kinetic parameters of a Haldane kinetic model. Indeed, even if the parameters are structurally identifiable like a Monod model (Aborhey and Williamson, 1978), the presence of uncertainty and noise as well as the number of experimental data, particularly over inhibition makes these parameters often practically unidentifiable (Dochain and Vanrolleghem, 2001). Thus, the set of parameters determined by an optimization method may not be unique. The method developed here from the literature aims at maximizing the accuracy of the obtained data. The estimation of the Haldane kinetic parameters was performed by minimizing an objective function considering the three measured state variables: the cumulative methane production, the methane flow rate, and the VFA concentration. This function has also considered arbitrarily chosen

weights to possibly balance the weight of one state variable over the others in the identification process. The objective function is defined in equation (25) as a function of the parameter set to be determined $p = [\mu_2^{max}; K_{S2}; K_I]$.

$$J(p) = \sum_{n=1}^{N} \Big[\sigma_1 \big(CH_{4,i}^{sim}(\hat{p}) - CH_{4,i}^{exp}\big)^T \big(CH_{4,i}^{sim}(\hat{p}) - CH_{4,i}^{exp}\big) + \sigma_2 \big(Q_{CH4,i}^{sim}(\hat{p}) - Q_{CH4,i}^{exp}\big)^T \big(Q_{CH4,i}^{sim}(\hat{p}) - Q_{CH4,i}^{exp}\big) + \sigma_3 \big(FOS_i^{sim}(\hat{p}) - FOS_i^{exp}\big)^T \big(FOS_i^{sim}(\hat{p}) - FOS_i^{exp}\big) \Big] \quad \textbf{(25)}$$

where J is the objective function. N represents the number of experimental points, and σ_1, σ_2 and σ_3 the weights assigned to each state variable, equal to 1, 0.5, and 2, respectively. An interior point optimization method was used to perform the nonlinear optimization of the objective function under constraints. The problem was solved with the SciIPOpt toolkit on Scilab 6.0 (ESI Group). The relative convergence tolerance was chosen equal to $1x10^{-3}$. The constraints and initialization for each kinetic parameter were found in the literature and arbitrarily chosen (Zaher et al., 2009; Müller et al., 2002). These data are illustrated in **Table 3**.

2.4.3 Sensitivity analysis and Conditioning of the objective function

The vector of the state variables studied for the calibration of Haldane kinetics depended on time, other state variables, and model parameters as shown in equation (26). The sensitivity of each parameter is defined by equation (27) and the model sensitivity matrix is determined by equation (28).

$$X = (CH_4, Q_{CH4}, FOS), \qquad p = (\mu_2^{max}, K_{S2}, K_I) \quad \textbf{(26)}$$

$$S(t) = \frac{\partial x}{\partial p} \quad \textbf{(27)}$$

$$\frac{\partial S(t)}{\partial t} = \frac{\partial f(t,x,p)}{\partial x} S + \frac{\partial f(t,x,p)}{\partial p}, \qquad \frac{\partial x}{\partial t} = f(t,x,p) \tag{28}$$

The determination of the sensitivity matrix allowed us to determine the sensitivity of the output variables for each input parameter of the calibration step. The calculations were performed using the complex-step derivation approximation method (Martin et al., 2003). Moreover, the approximation of the objective function allowed us to draw the curves of the function according to the values of the parameters to be determined and according to the domains of existence defined for these parameters. The objective function was plotted as a function of each pair of parameters to be determined in order to determine the quality of the conditioning of the objective function (Munack, 1989).

3 Results and discussion

3.1 Batch reactors performance

Mass balances were determined at the end of each experiment, with a minimal value of 96.1% attesting to the absence of local batch failures. The VS removal during these experiments was determined with an average value of $57.7 \pm 0.1\%$. During preliminary experiments, when substrates were not immersed in the liquid phase, a VS removal of 64% was observed with the same experiment duration. This observation could be explained by a strong VFA production at the beginning of experiments which could cause a temporary inhibition impacting the methane yield (Wollak *et al*., 2018). Accumulated methane yield and VFA concentration are represented in **Fig. 2** for each reactor. Two methane flow production peaks could be observed at the beginning and the end of the experiment. This behavior is typical of solid-state anaerobic digestion (André *et al*., 2015; Degueurce *et al*., 2016; Riggio *et al*., 2017) and the main challenge for solid-state anaerobic digestion is to consider this behavior in a mathematical model (Coutu *et al*., 2022). The experiment was stopped after 42 days to remain realistic about the real operating time of batch reactors and

to respect the usual industrial constraints. The accumulated methane yield reached was respectively 99.5% and 88.6% of the BMP measurement at the end of experiments for the reactors (R1) and (R2) attesting to great experimental conditions.

3.2 Identifiability of model parameters and unmonitored variables

Equations (14) and (18) were used on the results of the experiment (R2) to determine the values and standard deviations of the yield coefficients k_1^1 and k_1^2. Equation (14) was used to determine the k_1^2 coefficient in the stage where only MeM was consumed. This stage is identified in the experiment (R2) as stage 1 before the first injection of RJ. The coefficient k_1^1 was then identified over stage 2, representing the first RJ injection, using equation (18). All the results obtained are presented in **Table 3**. No outliers were observed during this step, with a value of k_1^1 obtained of 0.977 and a value of k_1^2 of 0.987.

In order to validate these values, the parameters k_1^1 and k_1^2 were determined with the same method using the results of the experiment (R1). The hypothesis was made that the experiment (R1) was divided into 2 stages: a first stage with degradation of both substrates and rapid degradation of the RJ, and a second stage where only the MeM was consumed. Equation (14) was used in the second stage of the experiment (R1) and equation (18) in the first stage. The values obtained were k_1^1=0.976 and k_1^2=0.987, which validated the calibration performed previously.

The values of parameters μ_1^1 and μ_1^2 were also obtained using equations (24) from the data obtained from the experiment (R2). μ_1^2 was first determined in stage 1 and then μ_1^1 was determined between each addition of RJ in stages 2 to 6. The values obtained for the calibration of these two parameters were $\mu_1^1=3.15.10^{-2}$ h^{-1} and $\mu_1^2=1.42.10^{-4}$ h^{-1}. To validate these results, μ_1^1 and μ_1^2 were also determined in the experiment (R1). The second identified stage of (R1) was used to determine μ_1^1 and then the first identified stage of (R1) was used to determine μ_1^2. The values

311 obtained were μ_1^1=1.68.10^{-2} h^{-1} and μ_1^2=1.44.10^{-4} h^{-1}. These values were of the same order of
312 magnitude as the values obtained during the calibration, which validated the calibration of the
313 parameters μ_1^1 and μ_1^2 from the experiment (R2).

314 In order to obtain the unmonitored variables in the experiment (R1), the reaction invariant notion
315 was also used (Dochain et al., 1992). The monitoring of these state variables allowed validation of
316 state variables simulated from the calibration data on the experiment (R1). Equations (21) and (22)
317 were used and the results obtained are presented in **Fig 3**.

318 ### *3.3 Calibration of Haldane kinetic parameters*

319 The calibration step of Haldane kinetic parameters aimed to obtain the best fitting with the
320 calibration data set of the experiment (R2). Two different data sets were used to calibrate and
321 validate this set of parameters through 3 state variables: the cumulated methane production, the
322 VFA concentration, and the methane flow rate observed respectively in experiments (R2) and (R1).
323 The calibration step was carried out by trial and error to obtain the best dataset possible. First of
324 all, a conditioning study of the objective function was done to determine if the objective function
325 was well-conditioned. Then a minimization procedure of the objective function was done using an
326 interior point optimization method.

327 #### *3.3.1 Conditioning of the objective function*

328 The study of the conditioning of the objective function allowed us to determine if the Haldane
329 kinetic parameters were identifiable. To perform this study, the value of the objective function
330 presented in equation (25) was determined by discretization by varying each parameter over the
331 calibration interval considered. The calibration interval is presented in **Table 3**. A discretization
332 step was arbitrarily chosen to divide the calibration interval into 20 equal parts for each parameter,
333 which represented 8000 estimations of the objective function. Once the values of the objective

function were obtained as a function of each set of parameters, the objective function was plotted as a function of the parameters associated in pairs. The result of this conditioning is presented in **Fig 4**. In these figures, it is evident that the objective function was ill-conditioned because the objective function as a function of each pair of parameters was represented by a very flattened ellipse (Dochain and Vanrolleghem, 2001). This first observation resulted in probably poor practical identifiability, which corroborated the assumptions made earlier. A sensitivity analysis was done following this conditioning study to determine which parameters were practically identifiable (Robinson et al., 1985).

3.3.2 Sensitivity analysis

In many biological models, kinetic parameters are highly correlated, which can result in "valley" behaviors in which several combinations of parameters can describe the same data similarly. It is therefore interesting to plot sensitivity functions to determine the practical identifiability of the studied model. The sensitivity analysis was here conducted by considering the impact of the three parameters to be determined on the three measured state variables present in the Haldane kinetics. The same curve shapes could be observed for the different parameters considered. This behavior could be observed for each state variable, which meant that the kinetic parameters were not identifiable and therefore there was not a unique solution for the set of parameters to be determined. Moreover, the sensitivity of each state variable to the K_I parameter was much lower than other parameters, with an order of magnitude of 10^{-8} against 10^{-4}. However, the presence of RJ injections allowed increasing the sensitivity of the different state variables to the parameters to be determined with a 10 factor. The consequence was an improvement in the identifiability of parameters during the calibration step. This phenomenon is consistent with the observations made in the literature (Vanrolleghem et al., 1995) and allowed to confirm the use of the data set from the experiment (R2) for the calibration step. Results of the sensitivity analysis are illustrated in **Fig**

5 for the cumulated methane production sensitivity to the K_{S2} parameter. Following this observation, the objective of the calibration step was to obtain the optimal set of parameters in order to fit the model with the experimental observations of (R2).

3.3.3 Calibration results

The calibration of Haldane kinetic parameters was done to obtain the best fitting with experimental results from the experiment (R2). This step was carried out by trial and error to find the best data set with optimal parameters. Calibration results are illustrated in **Fig 6**. The simulation results represented by continuous lines were close to the experimental data which were represented by dots. The Haldane kinetics obtained are presented in **Table 3**. These parameters values were very different from other studies in the literature. While μ_2^{max} was in line with the literature (Zaher et al., 2009; Müller et al., 2002), the K_{S2} calibration value was a little high and K_I was very low in comparison with values obtained from the literature. This difference in behavior could be explained by slower anaerobic digestion and the presence of inhibition phenomena specific to MeM and RJ.

3.4 Model validation

Validation steps were previously conducted on each parameter determination and a global validation was done considering experiment (R1). Results are illustrated in **Fig 6**. The simulation done correctly reproduced the global behavior of each solute for a complete period of 45 days. The main quality of this simplified model is the consideration of a low number of parameters, which allowed a faster and easier calibration step. However, the calibration step was very sensitive to the initialization step and parameter bounds, which could be validated by sensitivity analysis. Although the simulated curve representing VFA concentration was representative of the experimental data, the simulated methane yield showed a deviation from the experimental values. This deviation is

381 due to the presence of 2 peaks of methane production characteristic of the SS-AD. The model
382 developed in this paper allows the analysis of the behavior and evolution of the biomass and the
383 different chemical species present. The two peaks of methane production were modelized, which
384 is impossible with the usual models of the literature. This model is a first step to characterize
385 complex co-substrates as MeM and RJ with a simple model using few parameters but this model
386 could potentially evolve into a spatially distributed model introducing new parameters and using
387 new experiments to fit perfectly with the methane production curve.

388 *3.5 Discussion about possible inhibitions*

389 The specific behavior of MeM and RJ digestion could be due to high VFA concentrations (until 19
390 $g.L^{-1}$ during our preliminary experiments) (Khartikheyan and Visvanathan, 2013) or ammonia
391 concentrations (between 4 $g.L^{-1}$ and 5 $g.L^{-1}$ during our experiments). These values could be a source
392 of inhibition (Amani et al., 2010) but the acclimatization of the inoculum was carried out upstream,
393 which makes it possible not to impact the anaerobic digestion (Chen et al., 2008; Yenigun and
394 Demirel, 2013). Another possibility is an inhibition of sodium chloride (Feijoo et al., 1995) but just
395 like ammonia, the acclimatization of the inoculum was carried out upstream and there is no
396 possible impact on the methane yield (Kimata-Kino et al., 2011). The results obtained by this study
397 also showed that the released fluid has its importance in the SS-AD phenomenon and should not
398 be lost during MeM grinding. The potential presence of such inhibitions could modify the methane
399 yield and VFA accumulation curve shapes. Not all of these modifications were considered in the
400 mathematical model of this study and could potentially falsify the calibration results. Indeed, the
401 Haldane kinetics for Methanogenesis step used in this study considered inhibitions on
402 methanogenic biomass but inhibitions on other biomass were neglected and could potentially vary
403 the calibration results. In this study, the methane yields observed were consistent with the
404 literature (Wollak et al., 2018; Akizuki et al., 2016; Nkemka and Murto, 2013), attesting robust

405 experimental results to modeling the phenomenon of MeM and RJ SS-AD. However, further study
406 will be needed to improve the fit between the model and the experimental curves by better
407 characterizing the inhibitions of this process.

408 4 Conclusions

409 A simplified AM2 model was developed to characterize *Mytilus edulis* SS-AD. This model was
410 verified, implemented, and validated in 60L batch reactors in mesophilic conditions. A better
411 sensitivity with delayed substrate injections throughout the experiment with a factor of 10. These
412 results gave a correct approximation of solutes behavior with an accumulated methane yield
413 representing 88.6% of the BMP measurement, and a volatile removal of 57.7% attesting to great
414 experimental conditions. and could identify the two methane production peaks characteristics of
415 SS-AD but the results did not allow for prediction with enough accuracy to implement control tools
416 to optimize methane production. Further work is needed with new considerations to better
417 understand the phenomenon of *Mytilus edulis* solid-state anaerobic digestion. A further study
418 could be done to evolve this model into a spatially distributed model with more parameters in
419 order to fit perfectly with the methane production curve.

420 Acknowledgments

421 The authors gratefully thank Cultimer France, the ANRT, the region of Bretagne, the GALPA, and
422 the FEAMP for the support provided for this work and the Ph.D. grant of Maël Mercier-Huat. The
423 authors are very grateful to Rejanne Le Bivic for her carefully reading and English revision of the
424 manuscript.

425 References

426 Abbassi-Guendouz, A., Brockmann, D., Trably, E., Dumas, C., Delgenès, J.-P., Steyer, J.-P., Escudié, R., 2012. Total
427 solids content drives high solid anaerobic digestion via mass transfer limitation. Bioresour. Technol.
428 111, 55–61. https://doi.org/10.1016/j.biortech.2012.01.174

429 Aborhey, S., Williamson, D., 1978. State and parameter estimation of microbial growth processes. Automatica 14,
430 493–498. https://doi.org/10.1016/0005-1098(78)90008-0

431 Afrose, S., Hammershøj, M., Nørgaard, J.V., Engberg, R.M., Steenfeldt, S., 2016. Influence of blue mussel (Mytilus
432 edulis) and starfish (Asterias rubens) meals on production performance, egg quality and apparent total
433 tract digestibility of nutrients of laying hens. Anim. Feed Sci. Technol. 213, 108–117.
434 https://doi.org/10.1016/j.anifeedsci.2016.01.008

435 Akizuki, S., Matsuyama, T., Toda, T., 2016. An anaerobic-aerobic sequential batch system using simultaneous
436 organic and nitrogen removal to treat intermittently discharged organic solid wastes. Process Biochem.
437 51, 1264–1273. https://doi.org/10.1016/j.procbio.2016.05.011

438 Akizuki, S., Nagao, N., Toda, T., 2018. A multifunctional single-stage process for the effective methane recovery
439 and denitrification of intermittently discharged wastes. Int. Biodeterior. Biodegrad. 127, 201–208.
440 https://doi.org/10.1016/j.ibiod.2017.11.013

441 Amani, T., Nosrati, M., Sreekrishnan, T.R., 2010. Anaerobic digestion from the viewpoint of microbiological,
442 chemical, and operational aspects — a review. Environ. Rev. 18, 255–278. https://doi.org/10.1139/A10-
443 011

444 André, L., Durante, M., Pauss, A., Lespinard, O., Ribeiro, T., Lamy, E., 2015. Quantifying physical structure changes
445 and non-uniform water flow in cattle manure during dry anaerobic digestion process at lab scale:
446 Implication for biogas production. Bioresour. Technol. 192, 660–669.
447 https://doi.org/10.1016/j.biortech.2015.06.022

448 André, L., Pauss, A., Ribeiro, T., 2018. Solid anaerobic digestion: State-of-art, scientific and technological hurdles.
449 Bioresour. Technol. 247, 1027–1037. https://doi.org/10.1016/j.biortech.2017.09.003

450 Anwar, N., Wang, W., Zhang, J., Li, Y., Chen, C., Liu, G., Zhang, R., 2016. Effect of sodium salt on anaerobic
451 digestion of kitchen waste. Water Sci. Technol. 73, 1865–1871. https://doi.org/10.2166/wst.2016.035

452 APHA, 1998. Standard Methods for the Examination of Water and Wastewater. American Public Health
453 Association, 20th ed. American water works association and water environment federation,
454 Washington, USA.

455 Batstone, D.J., Keller, J., Angelidaki, I., Kalyuzhnyi, S.V., Pavlostathis, S.G., Rozzi, A., Sanders, W.T.M., Siegrist, H.,
456 Vavilin, V.A., 2002. The IWA Anaerobic Digestion Model No 1 (ADM1). Water Sci. Technol. 45, 65–73.
457 https://doi.org/10.2166/wst.2002.0292

458 Bernard, O., Hadj-Sadok, Z., Dochain, D., Genovesi, A., Steyer, J.-P., 2001. Dynamical model development and
459 parameter identification for an anaerobic wastewater treatment process. Biotechnol. Bioeng. 75, 424–
460 438. https://doi.org/10.1002/bit.10036

Bollon, J., Le-hyaric, R., Benbelkacem, H., Buffiere, P., 2011. Development of a kinetic model for anaerobic dry digestion processes: Focus on acetate degradation and moisture content. Biochem. Eng. J. 56, 212–218. https://doi.org/10.1016/j.bej.2011.06.011

Chen, Y., Cheng, J.J., Creamer, K.S., 2008. Inhibition of anaerobic digestion process: A review. Bioresour. Technol. 99, 4044–4064. https://doi.org/10.1016/j.biortech.2007.01.057

Coutu, A., Hernández-Shek, M.A., Mottelet, S., Guérin, S., Rocher, V., Pauss, A., Ribeiro, T., 2022. A coupling model for solid-state anaerobic digestion in leach-bed reactors: Mobile-Immobile water and anaerobic digestion model. Bioresour. Technol. Rep. 17, 100961. https://doi.org/10.1016/j.biteb.2022.100961

Degueurce A., Tremier A., Peu P., 2016. Dynamic effect of leachate recirculation on batch mode solid state anaerobic digestion: Influence of recirculated volume, leachate to substrate ratio and recirculation periodicity. Bioresour. Technol. 216, 553–561. https://doi.org/10.1016/j.biortech.2016.05.113

DiLoreto, Z.A., Weber, P.A., Olds, W., Pope, J., Trumm, D., Chaganti, S.R., Heath, D.D., Weisener, C.G., 2016. Novel cost-effective full-scale mussel shell bioreactors for metal removal and acid neutralization. J. Environ. Manage. 183, 601–612. https://doi.org/10.1016/j.jenvman.2016.09.023

Dochain, D., Perrier, M., Ydstie, B.E., 1992. Asymptotic observers for stirred tank reactors. Chem. Eng. Sci. 47, 4167–4177. https://doi.org/10.1016/0009-2509(92)85166-9

Dochain, D., Vanrolleghem, P., 2001. Dynamical Modelling and Estimation in Wastewater Treatment Processes, IWA Publishing.

Donoso-Bravo, A., Mailier, J., Martin, C., Rodríguez, J., Aceves-Lara, C.A., Wouwer, A.V., 2011. Model selection, identification and validation in anaerobic digestion: A review. Water Res. 45, 5347–5364. https://doi.org/10.1016/j.watres.2011.08.059

Du, M., Liu, X., Wang, D., Yang, Q., Duan, A., Chen, H., Liu, Y., Wang, Q., Ni, B.-J., 2021. Understanding the fate and impact of capsaicin in anaerobic co-digestion of food waste and waste activated sludge. Water Res. 188, 116539. https://doi.org/10.1016/j.watres.2020.116539

FAO, 2020. FAO Yearbook. Fishery and Aquaculture Statistics 2019. https://www.fao.org/fishery/en/publications/287024 (accessed 2.16.22).

Fdez.-Güelfo, L.A., Álvarez-Gallego, C., Sales Márquez, D., Romero García, L.I., 2011. Dry-thermophilic anaerobic digestion of simulated organic fraction of Municipal Solid Waste: Process modeling. Bioresour. Technol. 102, 606–611. https://doi.org/10.1016/j.biortech.2010.07.124

Feijoo, G., Soto, M., Méndez, R., Lema, J.M., 1995. Sodium inhibition in the anaerobic digestion process: Antagonism and adaptation phenomena. Enzyme Microb. Technol. 17, 180–188. https://doi.org/10.1016/0141-0229(94)00011-F

Fernández-Calviño, D., Cutillas-Barreiro, L., Nóvoa-Muñoz, J.C., Díaz-Raviña, M., Fernández-Sanjurjo, M.J., Álvarez-Rodríguez, E., Núñez-Delgado, A., Arias-Estévez, M., Rousk, J., 2018. Using pine bark and mussel shell

amendments to reclaim microbial functions in a Cu polluted acid mine soil. Appl. Soil Ecol. 127, 102–111. https://doi.org/10.1016/j.apsoil.2018.03.010

Fernández-Calviño, D., Garrido-Rodríguez, B., Arias-Estévez, M., Díaz-Raviña, M., Álvarez-Rodríguez, E., Fernández-Sanjurjo, M.J., Nuñez-Delgado, A., 2015. Effect of crushed mussel shell addition on bacterial growth in acid polluted soils. Appl. Soil Ecol. 85, 65–68. https://doi.org/10.1016/j.apsoil.2014.09.010

Gavala, H.N., Angelidaki, I., Ahring, B.K., 2003. Kinetics and Modeling of Anaerobic Digestion Process, in: Ahring, B.K., Angelidaki, I., de Macario, E.C., Gavala, H. N., Hofman-Bang, J., Macario, A.J.L., Elferink, S.J.W.H.O., Raskin, L., Stams, A.J.M., Westermann, P., Zheng, D. (Eds.), Biomethanation I, Advances in Biochemical Engineering/Biotechnology. Springer, Berlin, Heidelberg, pp. 57–93. https://doi.org/10.1007/3-540-45839-5_3

Holliger, C., Alves, M., Andrade, D., Angelidaki, I., Astals, S., Baier, U., Bougrier, C., Buffière, P., Carballa, M., de Wilde, V., Ebertseder, F., Fernández, B., Ficara, E., Fotidis, I., Frigon, J.-C., de Laclos, H.F., Ghasimi, D.S.M., Hack, G., Hartel, M., Heerenklage, J., Horvath, I.S., Jenicek, P., Koch, K., Krautwald, J., Lizasoain, J., Liu, J., Mosberger, L., Nistor, M., Oechsner, H., Oliveira, J.V., Paterson, M., Pauss, A., Pommier, S., Porqueddu, I., Raposo, F., Ribeiro, T., Rüsch Pfund, F., Strömberg, S., Torrijos, M., van Eekert, M., van Lier, J., Wedwitschka, H., Wierinck, I., 2016. Towards a standardization of biomethane potential tests. Water Sci. Technol.74, 2515–2522. https://doi.org/10.2166/wst.2016.336

Karthikeyan, O.P., Visvanathan, C., 2013. Bio-energy recovery from high-solid organic substrates by dry anaerobic bio-conversion processes: a review. Rev. Environ. Sci. Bio/Technol. 12, 257–284. https://doi.org/10.1007/s11157-012-9304-9

Kimata-Kino, N., Ikeda, S., Kurosawa, N., Toda, T., 2011. Saline adaptation of granules in mesophilic UASB reactors. Int. Biodeterior. Biodegrad. 65, 65–72. https://doi.org/10.1016/j.ibiod.2010.09.002

Kothari, R., Pandey, A.K., Kumar, S., Tyagi, V.V., Tyagi, S.K., 2014. Different aspects of dry anaerobic digestion for bio-energy: An overview. Renew. Sust. Energ. Rev. 39, 174–195. https://doi.org/10.1016/j.rser.2014.07.011

Li, Y., Park, S.Y., Zhu, J., 2011. Solid-state anaerobic digestion for methane production from organic waste. Renew. Sust. Energ. Rev. 15, 821–826. https://doi.org/10.1016/j.rser.2010.07.042

Liu, X., Coutu, A., Mottelet, S., Pauss, A., Ribeiro, T., 2023. Overview of Numerical Simulation of Solid-State Anaerobic Digestion Considering Hydrodynamic Behaviors, Phenomena of Transfer, Biochemical Kinetics and Statistical Approaches. Energies 16, 1108. https://doi.org/10.3390/en16031108

Martínez-García, C., González-Fonteboa, B., Carro-López, D., Martínez-Abella, F., 2019. Design and properties of cement coating with mussel shell fine aggregate. Constr. Build. Mater. 215, 494–507. https://doi.org/10.1016/j.conbuildmat.2019.04.211

528 Martínez-García, C., González-Fonteboa, B., Carro-López, D., Pérez-Ordóñez, J.L., 2020. Mussel shells: A canning
529 industry by-product converted into a bio-based insulation material. J. Clean. Prod. 269, 122343.
530 https://doi.org/10.1016/j.jclepro.2020.122343

531 Messiga, A.J., Sharifi, M., McVicar, K., Cheema, M., Hammermeister, A., 2016. Mussel's post-harvest washing
532 sediments consistency over time, and contribution to plant growth and nutrient uptake. J. Clean. Prod.
533 113, 216–223. https://doi.org/10.1016/j.jclepro.2015.11.062

534 Müller, T.G., Noykova, N., Gyllenberg, M., Timmer, J., 2002. Parameter identification in dynamical models of
535 anaerobic waste water treatment. Math. Biosci. 177–178, 147–160. https://doi.org/10.1016/S0025-
536 5564(01)00098-0

537 Munack, A., 1989. Optimal Feeding Strategy for Identification of Monod-Type Models by Fed-Batch Experiments,
538 in: Fish, N.M., Fox, R.I., Thornhill, N.F. (Eds.), Computer Applications in Fermentation Technology:
539 Modelling and Control of Biotechnological Processes. Springer Netherlands, Dordrecht, pp. 195–204.
540 https://doi.org/10.1007/978-94-009-1141-3_21

541 Murto, M., Björnsson, L., Mattiasson, B., 2004. Impact of food industrial waste on anaerobic co-digestion of
542 sewage sludge and pig manure. J. Environ. Manage. 70, 101–107.
543 https://doi.org/10.1016/j.jenvman.2003.11.001

544 Naik, A.S., Hayes, M., 2019. Bioprocessing of mussel by-products for value added ingredients. Trends Food Sci.
545 Technol. 92, 111–121. https://doi.org/10.1016/j.tifs.2019.08.013

546 Nkemka, V.N., Murto, M., 2013. Two-stage anaerobic dry digestion of blue mussel and reed. Renew. Energ. 50,
547 359–364. https://doi.org/10.1016/j.renene.2012.06.041

548 Pintado, J., Guyot, J.P., Raimbault, M., 1999. Lactic acid production from mussel processing wastes with an
549 amylolytic bacterial strain. Enzyme Microb. Technol. 24, 590–598. https://doi.org/10.1016/S0141-
550 0229(98)00168-9

551 Riggio, S., Torrijos, M., Debord, R., Esposito, G., van Hullebusch, E.D., Steyer, J.P., Escudié, R., 2017. Mesophilic
552 anaerobic digestion of several types of spent livestock bedding in a batch leach-bed reactor: substrate
553 characterization and process performance. Waste Manage. 59, 129–139.
554 https://doi.org/10.1016/j.wasman.2016.10.027

555 Robinson, J.A., 1985. Determining Microbial Kinetic Parameters Using Nonlinear Regression Analysis, in: Marshall,
556 K.C. (Ed.), Advances in Microbial Ecology: Volume 8, Advances in Microbial Ecology. Springer US,
557 Boston, MA, pp. 61–114. https://doi.org/10.1007/978-1-4615-9412-3_2

558 Sardenne, F., Forget, N., McKindsey, C.W., 2019. Contribution of mussel fall-off from aquaculture to wild lobster
559 Homarus americanus diets. Mar. Environ. Res. 149, 126–136.
560 https://doi.org/10.1016/j.marenvres.2019.06.003

561 Seco, N., Fernández-Sanjurjo, M.J., Núñez-Delgado, A., Alvarez, E., 2014. Spreading of mixtures including wastes
562 from the mussel shell treatment industry on an acid soil: effects on the dissolved aluminum species and
563 on pasture production. Journal of Cleaner Production 70, 154–163.Siegert, I., Banks, C., 2005. The effect
564 of volatile fatty acid additions on the anaerobic digestion of cellulose and glucose in batch reactors.
565 Process Biochem. 40, 3412–3418. https://doi.org/10.1016/j.procbio.2005.01.025

566 Vanrolleghem, P.A., Daele, M.V., Dochain, D., 1995. Practical identifiability of a biokinetic model of activated
567 sludge respiration. Water Res. 29, 2561–2570. https://doi.org/10.1016/0043-1354(95)00105-T

568 Vareltzis, P.K., Undeland, I., 2012. Protein isolation from blue mussels (Mytilus edulis) using an acid and alkaline
569 solubilisation technique—process characteristics and functionality of the isolates. J. Sci. Food Agric. 92,
570 3055–3064. https://doi.org/10.1002/jsfa.5723

571 Vijaykrishnaraj, M., Roopa, B.S., Prabhasankar, P., 2016. Preparation of gluten free bread enriched with green
572 mussel (Perna canaliculus) protein hydrolysates and characterization of peptides responsible for mussel
573 flavour. Food Chem. 211, 715–725. https://doi.org/10.1016/j.foodchem.2016.05.094

574 Wollak, B., Forss, J., Welander, U., 2018. Evaluation of blue mussels (Mytilus edulis) as substrate for biogas
575 production in Kalmar County (Sweden). Biomass Bioenerg. 111, 96–102.
576 https://doi.org/10.1016/j.biombioe.2018.02.008

577 Xu, F., Li, Y., Wang, Z.-W., 2015. Mathematical modeling of solid-state anaerobic digestion. Prog. Energ. Combust.
578 Sci. 51, 49–66. https://doi.org/10.1016/j.pecs.2015.09.001

579 Yenigün, O., Demirel, B., 2013. Ammonia inhibition in anaerobic digestion: A review. Process Biochem. 48, 901–
580 911. https://doi.org/10.1016/j.procbio.2013.04.012

581 Zaher, U., Li, R., Jeppsson, U., Steyer, J.-P., Chen, S., 2009. GISCOD: General Integrated Solid Waste Co-Digestion
582 model. Water Res. 43, 2717–2727. https://doi.org/10.1016/j.watres.2009.03.018

583 Zhang, H., Xia, W., Xu, Y., Jiang, Q., Wang, C., Wang, W., 2013. Effects of spray-drying operational parameters on
584 the quality of freshwater mussel powder. Food Bioprod. Process. 91, 242–248.
585 https://doi.org/10.1016/j.fbp.2012.10.006

586 Zhang, Y., Li, L., Kong, X., Zhen, F., Wang, Z., Sun, Y., Dong, P., lv, P., 2017. Inhibition Effect of Sodium
587 Concentrations on the Anaerobic Digestion Performance of Sargassum Species. Energ. Fuel. 31, 9.
588 https://doi.org/10.1021/acs.energyfuels.7b00557

589 Zhou, H., Ying, Z., Cao, Z., Liu, Z., Zhang, Z., Liu, W., 2020. Feeding control of anaerobic co-digestion of waste
590 activated sludge and corn silage performed by rule-based PID control with ADM1. Waste Manage. 103,
591 22–31. https://doi.org/10.1016/j.wasman.2019.12.021

592

593 **Figure captions**

Fig 1. Schematic representation of the experimentation set up

Fig 2. Solid-state anaerobic digestion performance on experiment (R1) with A : cumulated methane production, B: VFA concentration and C: methane flow rate and experiment (R2) with D : cumulated methane production, E: VFA concentration and F: methane flow rate and experiment. Different considered stages are represented on each experiment in blue and red zones

Fig 3. Unmonitored substrate concentrations of MeM and RJ all along SS-AD

Fig 4. Conditioning study of the objective function for each pair of parameters with A : μ_2^{max} and K_{S2}, B : K_I and K_{S2} and C : μ_2^{max} and K_I

Fig 5. Results of sensitivity analysis concerning the cumulated methane production sensitivity to K_{S2} parameter

Fig 6. A: Calibration step on A: cumulated methane production and VFA concentration, B: methane flow rate and Validation step on C: cumulated methane production and VFA concentration and D: methane flow rate; dots for average experimental values, lines for simulated values

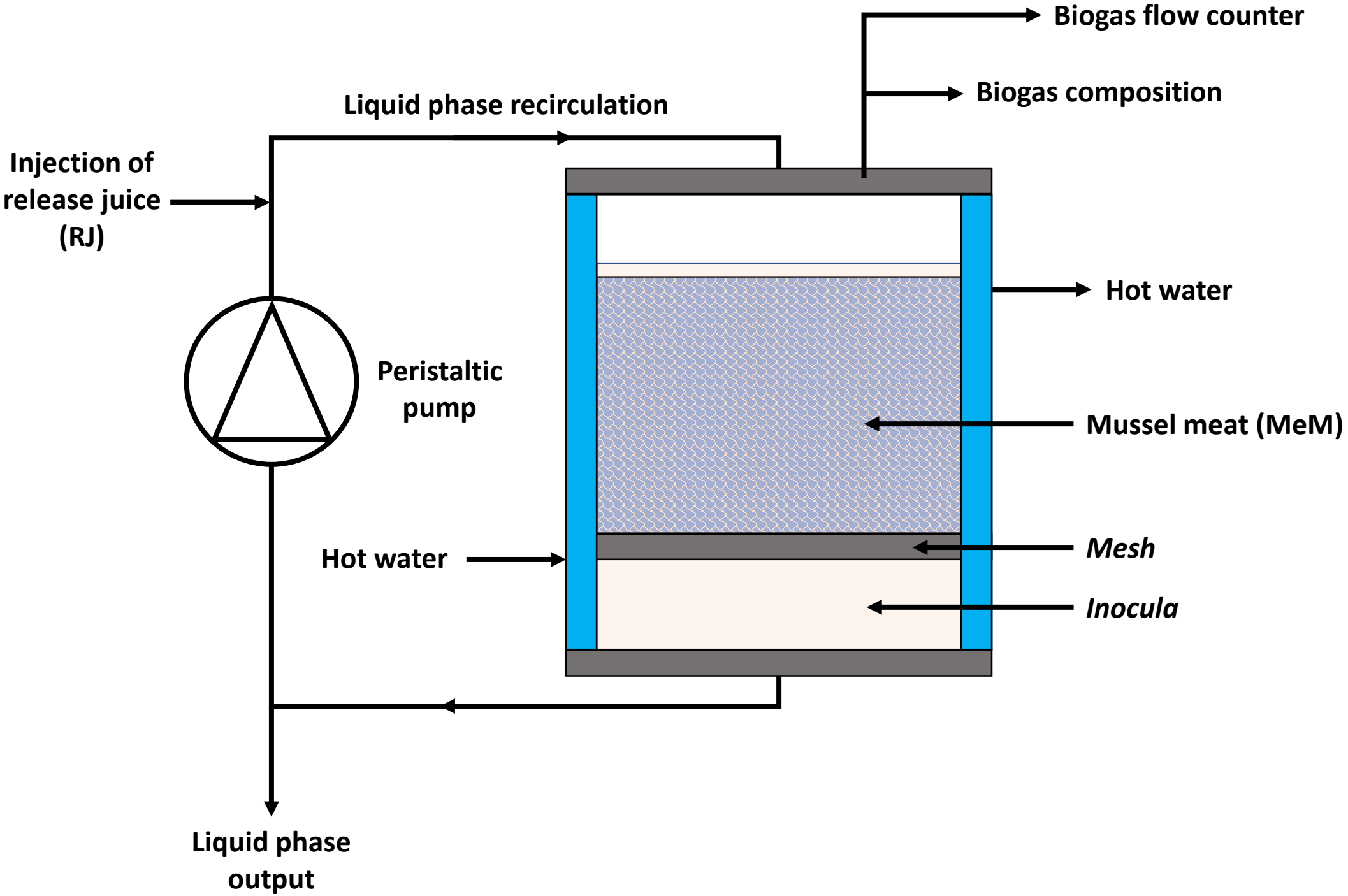
Biogas flow counter
Biogas composition
Liquid phase recirculation
Injection of release juice (RJ)
Hot water
Peristaltic pump
Mussel meat (MeM)
Hot water
Mesh
Inocula
Liquid phase output

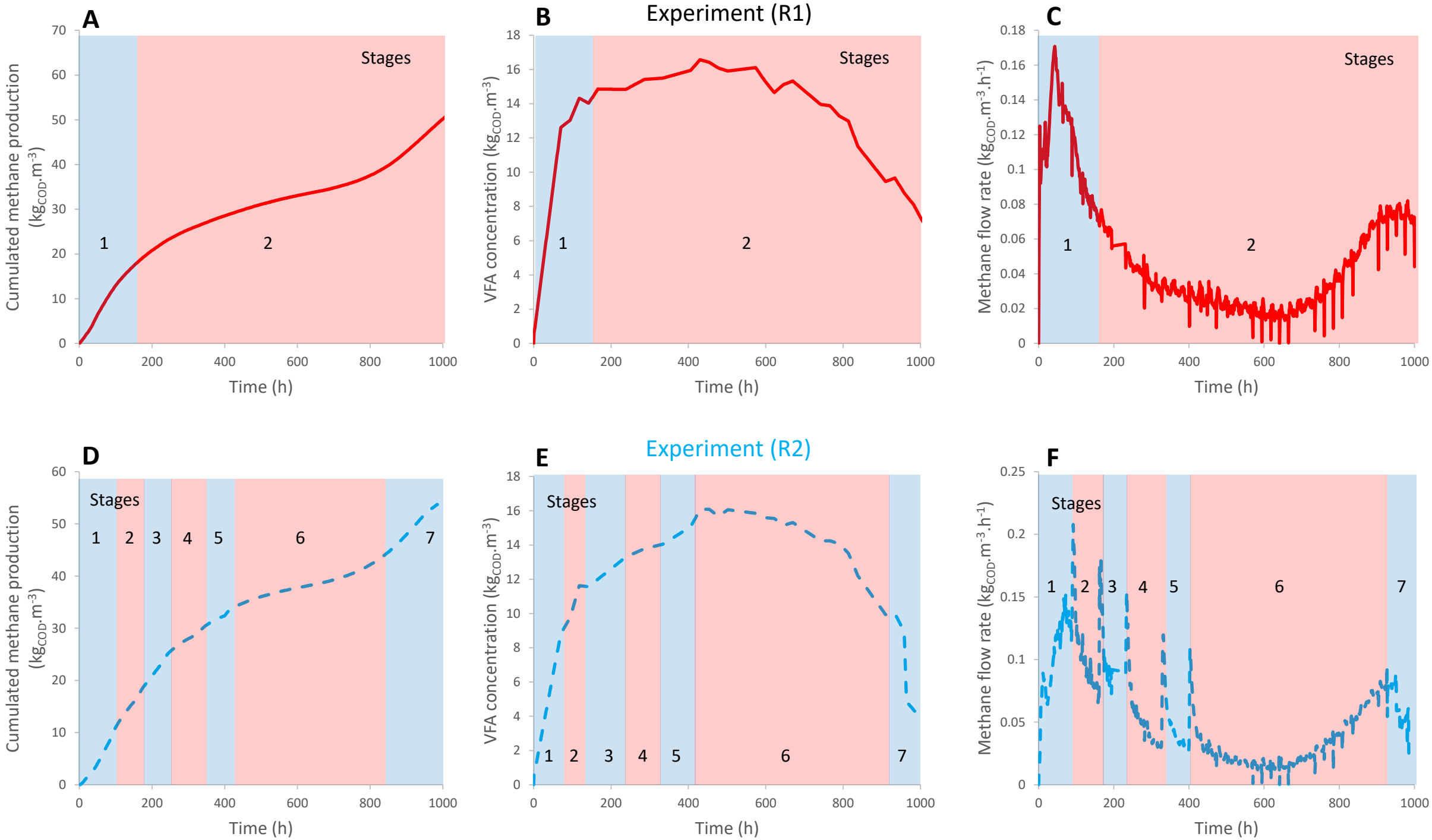
A
Cumulated methane production (kg$_{COD}$.m^{-3})
Stages
1
2
Time (h)
B
Experiment (R1)
VFA concentration (kg$_{COD}$.m^{-3})
Stages
1
2
Time (h)
C
Methane flow rate (kg$_{COD}$.m^{-3}.h^{-1})
Stages
1
2
Time (h)
D
Cumulated methane production (kg$_{COD}$.m^{-3})
Stages
1 2 3 4 5 6 7
Time (h)
E
Experiment (R2)
VFA concentration (kg$_{COD}$.m^{-3})
Stages
1 2 3 4 5 6 7
Time (h)
F
Methane flow rate (kg$_{COD}$.m^{-3}.h^{-1})
Stages
1 2 3 4 5 6 7
Time (h)

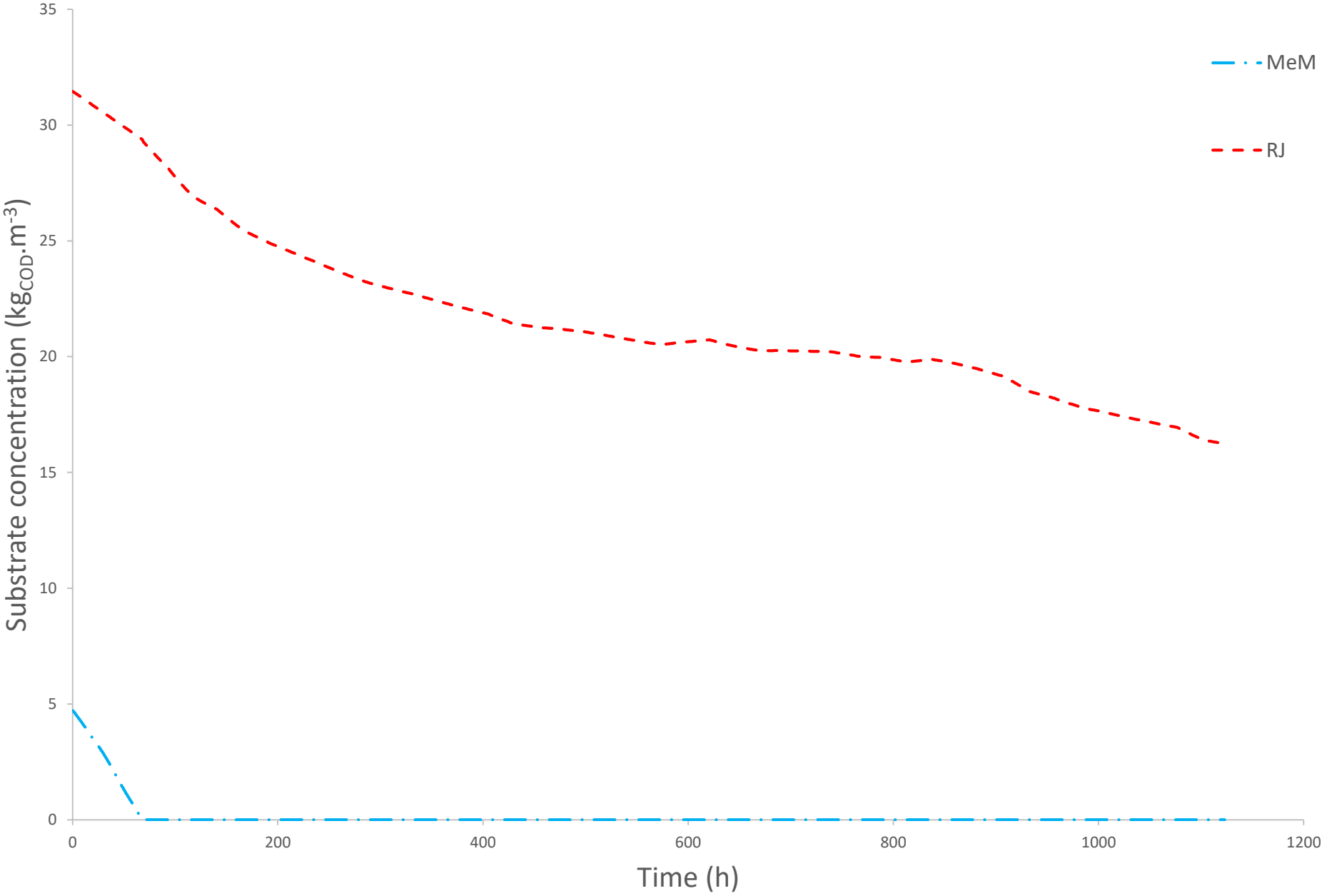
MeM
RJ
Substrate concentration (kg$_{COD}$.m^{-3})
Time (h)
0
5
10
15
20
25
30
35
0
200
400
600
800
1000
1200

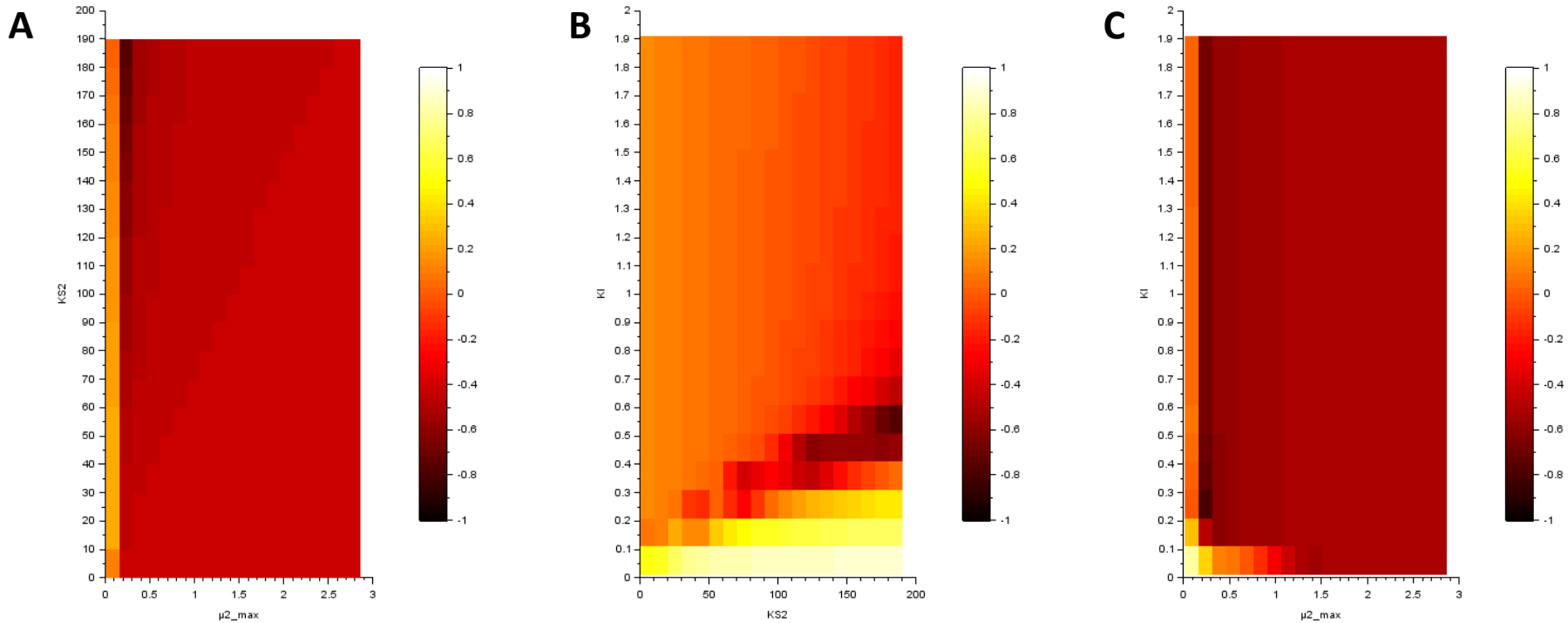
A
KS2
μ2_max
B
KI
KS2
C
KI
μ2_max

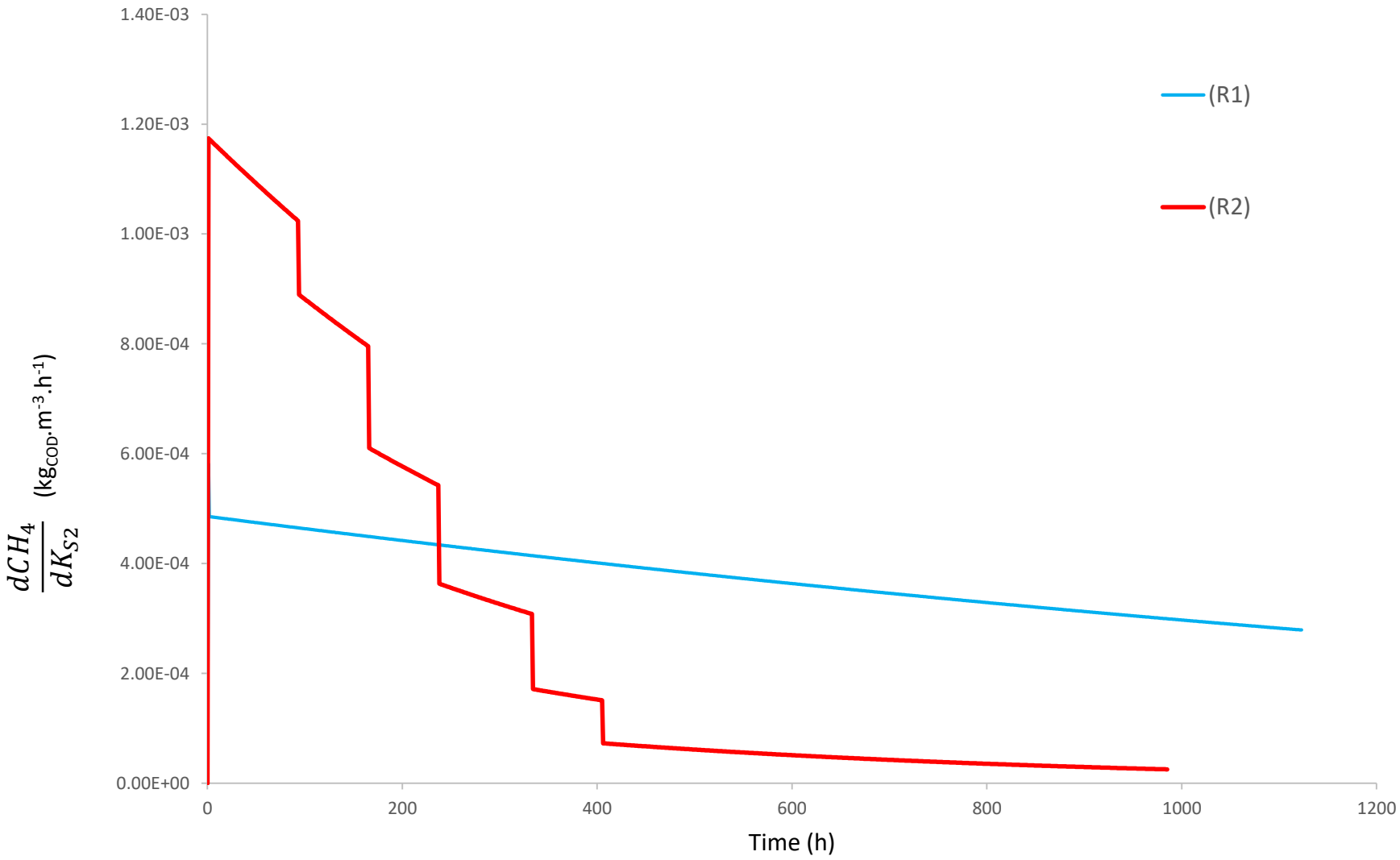
1.40E-03
1.20E-03
1.00E-03
8.00E-04
6.00E-04
4.00E-04
2.00E-04
0.00E+00
0
200
400
600
800
1000
1200
Time (h)
(R1)
(R2)
$\frac{dCH_4}{dK_{S2}}$ ($kg_{COD}.m^{-3}.h^{-1}$)

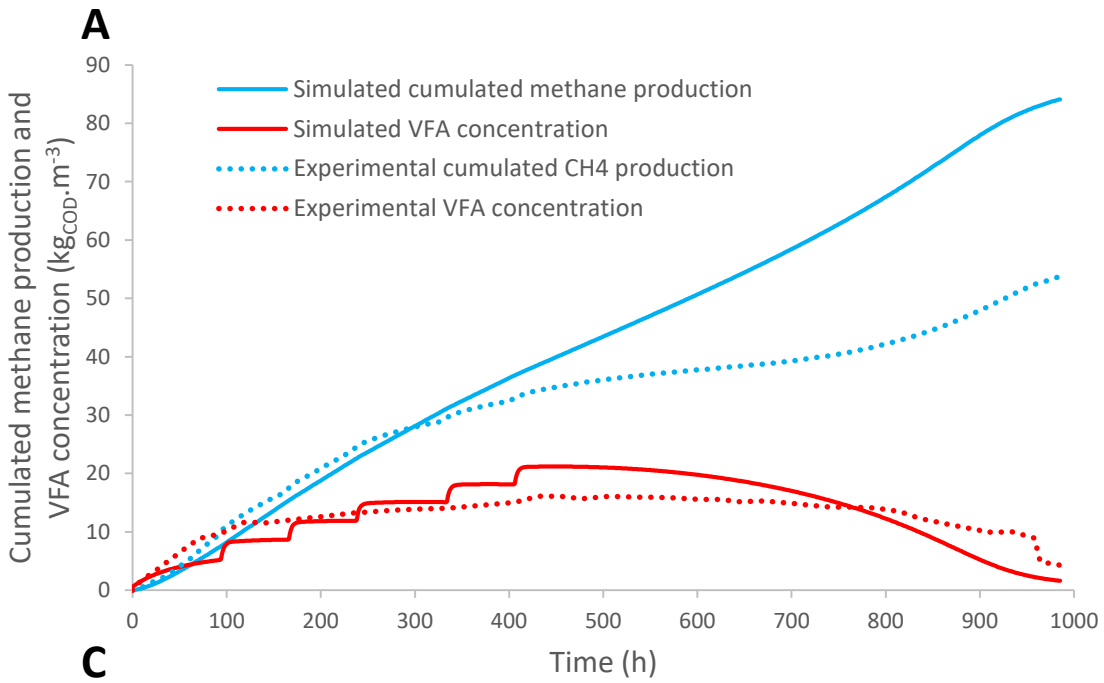
A
Simulated cumulated methane production
Simulated VFA concentration
Experimental cumulated CH4 production
Experimental VFA concentration
Cumulated methane production and VFA concentration (kgCOD.m-3)
Time (h)

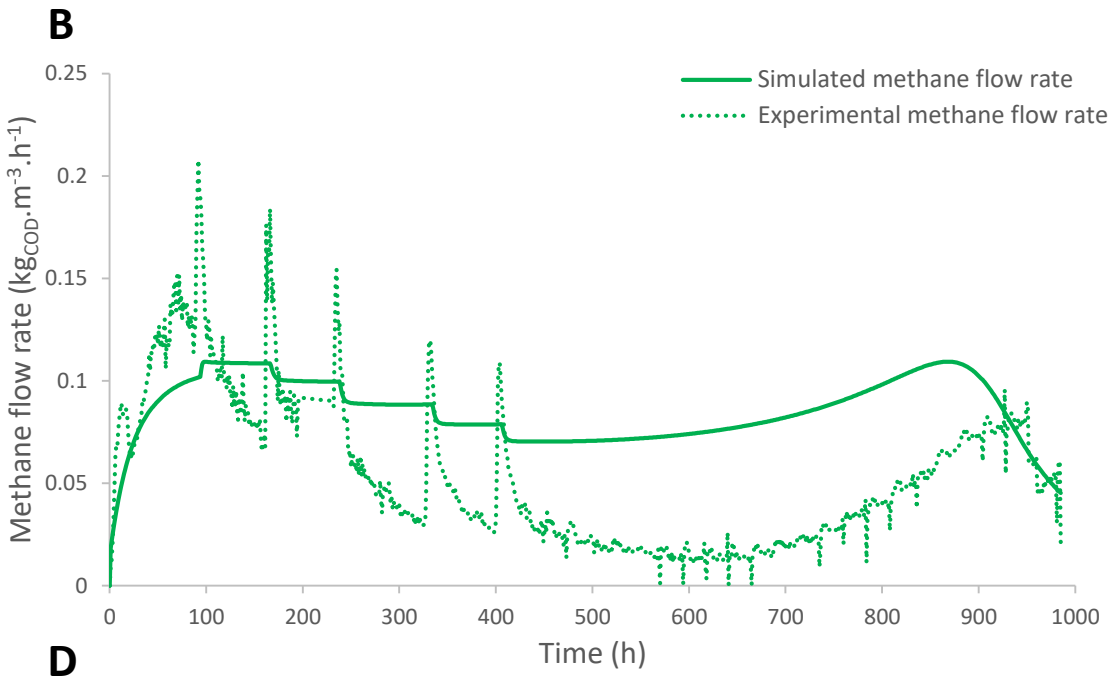
B
Simulated methane flow rate
Experimental methane flow rate
Methane flow rate (kgCOD.m-3.h-1)
Time (h)

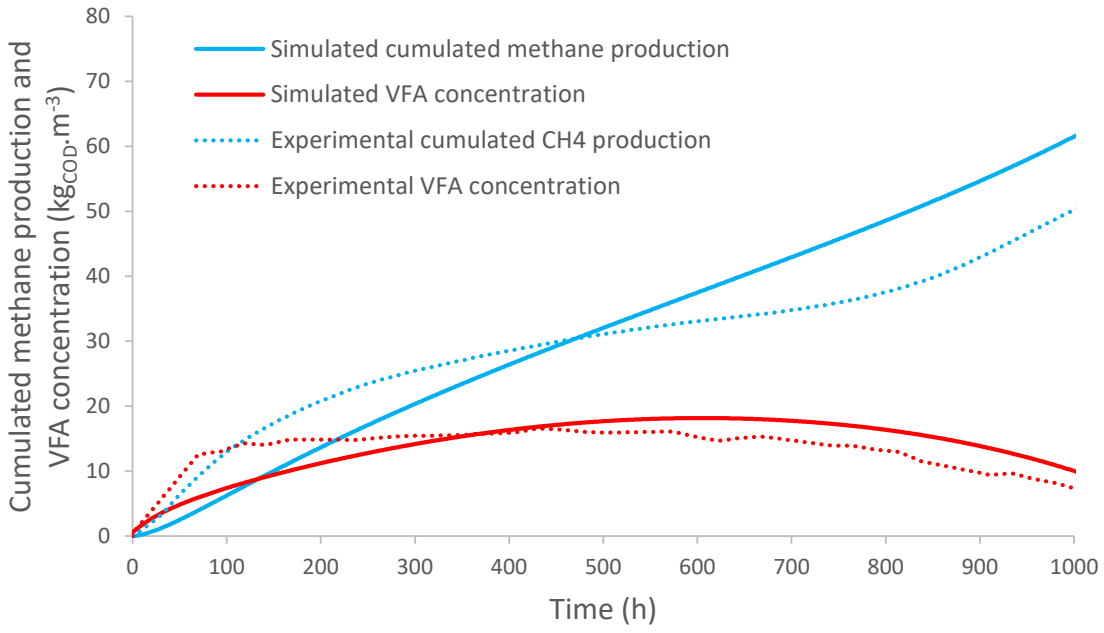
C
Simulated cumulated methane production
Simulated VFA concentration
Experimental cumulated CH4 production
Experimental VFA concentration
Cumulated methane production and VFA concentration (kgCOD.m-3)
Time (h)

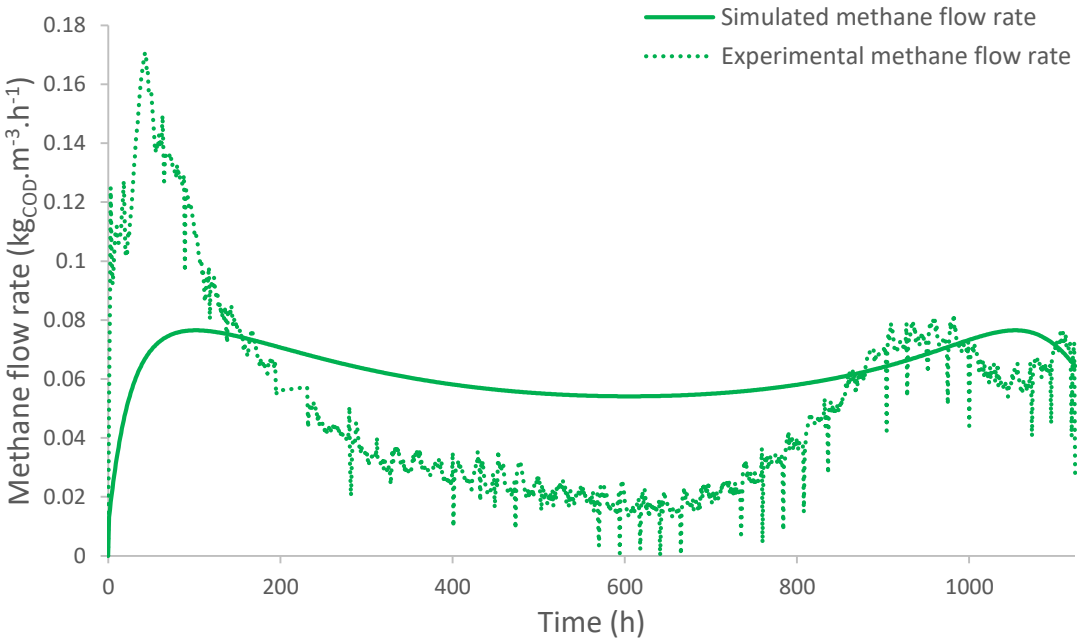
D
Simulated methane flow rate
Experimental methane flow rate
Methane flow rate (kgCOD.m-3.h-1)
Time (h)

Table 1 Chemical characteristics of inoculum and substrates used

		Run 1			Run 2		
	Unit	**Initial MeM**	**Initial RJ**	**Initial LM**	**Initial MeM**	**Initial RJ**	**Initial LM**
TS	%	67.2 ± 0.1	8.2 ± 0.1	3.8 ± 0.1	68.8 ± 1.6	12.4 ± 0.3	2.6 ± 0.1
VS	$\%_{TS}$	14.5 ± 0.5	62.4 ± 0.1	62.9 ± 0.2	12.2 ± 1.5	75.5 ± 0.7	51.5 ± 0.3
pH	-	-	5.3 ± 0.1	8.2 ± 0.1	-	5.7 ± 0.1	8.1 ± 0.1
VFA	$g_{HAc}.L^{-1}$	-	8.5 ± 0.4	0.05 ± 0.05	-	5.0 ± 0.1	0.0 ± 0.1
TAC	$g_{CaCO3}.L^{-1}$	-	0.2 ± 0.2	3.9 ± 0.1	-	0.05 ± 0.05	6.7 ± 0.1
BMP	$NL_{CH4}.kg_{VS}^{-1}$	277 ± 11	306 ± 8	-	277 ± 11	306 ± 8	-

Table 2 Peterson matrix of the model kinetics

Step	S_1^1	S_1^2	S_2	X_1	CH_4	Reaction rate
DHA - MeM	-1		k_1^1	$(1-k_1^1)$		$r_1^1 = \mu_1^1 S_1^1 X_1$
DHA - RJ		-1	k_1^2	$(1-k_1^2)$		$r_1^2 = \mu_1^2 S_1^2 X_1$
Methanogenesis			-1		k_2	$r_2 = \mu_2^{max} \frac{S_2 X_2}{S_2 + K_{S2} + \frac{S_2}{K_I}}$

Table 3 Kinetic parameters initialization and values obtained from calibration step

Parameter	Initialization value	Calibration value	Interval	Unit
k_1^1	-	0.976 ± 0.001	-	$-$
k_1^2	-	0.987 ± 0.001	-	$-$
μ_1^1	-	3.150 ± 1.068	-	$10^{-2}.h^{-1}$
μ_1^2	-	1.422 ± 1.313	-	$10^{-4}.h^{-1}$
μ_2^{max}	2.670	12.46 ± 1.204	[0.1 – 30]	$10^{-2}.h^{-1}$
K_{S2}	3.450	145.3 ± 12.67	[0.1 – 200]	$\mathrm{kg}_{COD}.\mathrm{L}^{-1}$
K_I	1.440	0.401 ± 0.061	[0.1 – 50]	$\mathrm{kg}_{COD}.\mathrm{L}^{-1}$

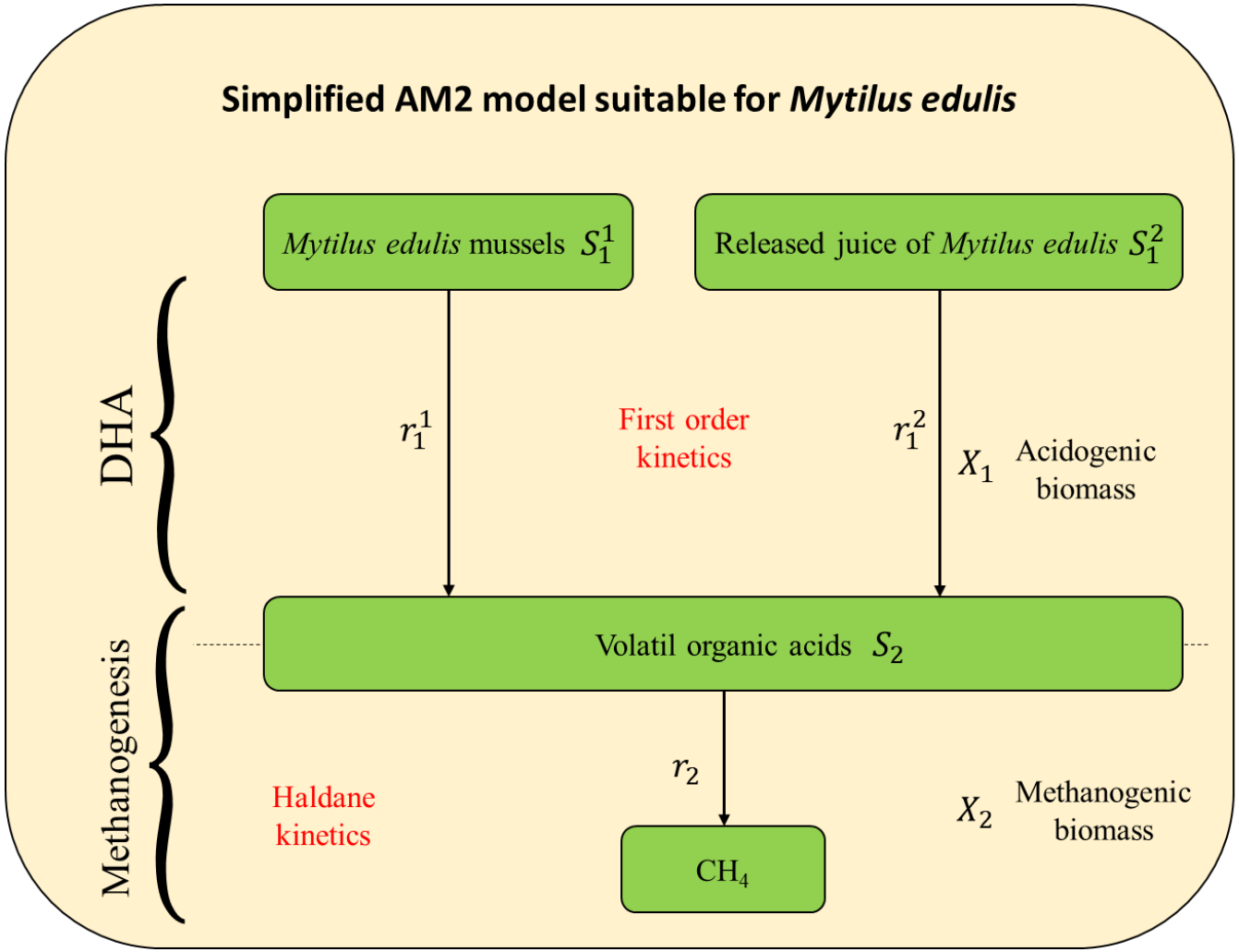
Simplified AM2 model suitable for *Mytilus edulis*
Mytilus edulis mussels S_1^1
Released juice of *Mytilus edulis* S_1^2
DHA
r_1^1
First order kinetics
r_1^2
X_1 Acidogenic biomass
Volatil organic acids S_2
Methanogenesis
r_2
Haldane kinetics
X_2 Methanogenic biomass
CH_4

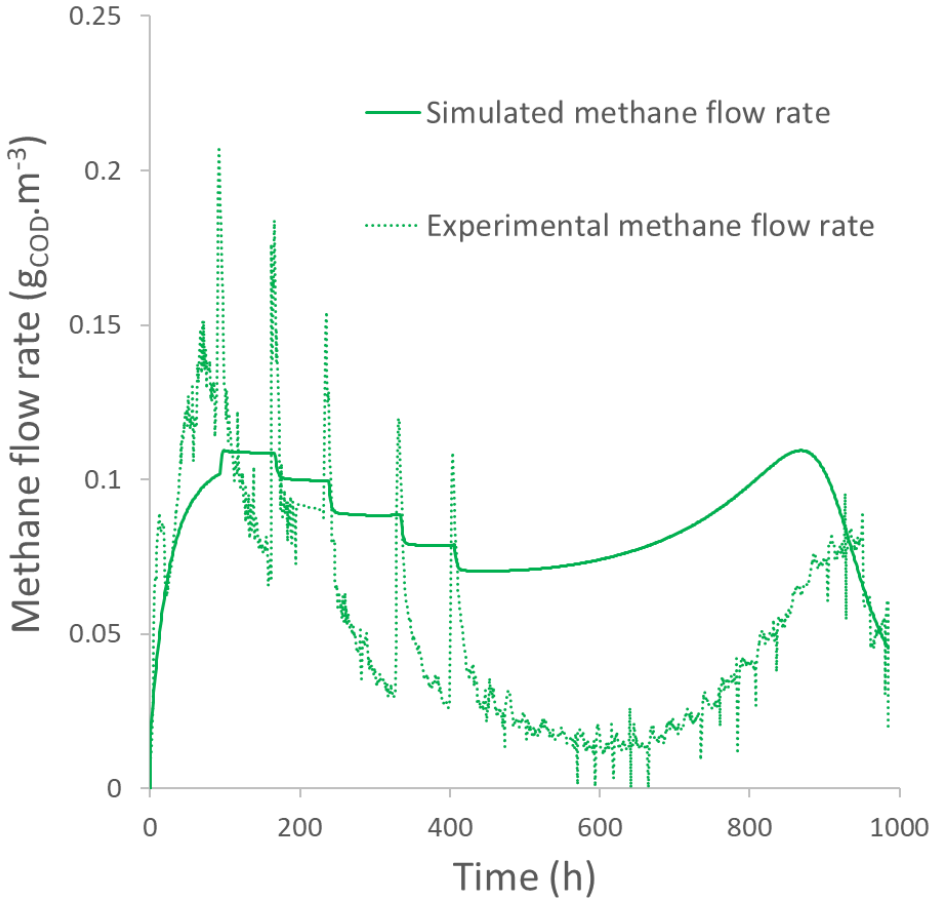
Simulated methane flow rate
Experimental methane flow rate
Methane flow rate ($g_{COD}.m^{-3}$)
0.25
0.2
0.15
0.1
0.05
0
0
200
400
600
800
1000
Time (h)